Available online at www.sciencedirect.com

ScienceDirect

IFAC PapersOnline CONFERENCE PAPER ARCHIVE

IFAC PapersOnLine 56-2 (2023) 5632–5636

Influence of the patient-specific structural prior mask on image reconstruction using the discrete cosine transform-based EIT algorithm

Rongqing Chen [*,**] **Alberto Battistel** [*] **Sabine Krueger-Ziolek** [*] **Erik Stein** [*] **Katharine Fairbairn** [***] **James Geoffrey Chase** [****] **Stefan J. Rupitsch** [**] **Knut Moeller** [*]

[*] *Institute for Technical Medicine (ITeM), Hochschule Furtwangen, Jakob-Kienzle-Straße 17, Villingen-Schwenningen, Germany (e-mail: rongqing.chen@hs-furtwangen.de).*

[**] *Faculty of Engineering, University of Freiburg, Georges-Köhler-Allee 101, Freiburg, Germany*

[***] *James Watt School of Engineering, University of Glasgow, Glasgow, G12 8QQ, United Kingdom*

[****] *Department of Mechanical Engineering, University of Canterbury, Private Bag 4800, Christchurch 8140, New Zealand*

Abstract: Electrical impedance tomography (EIT) is an imaging technology but suffers greatly from the ill-posed inverse problem when reconstructing an image, which is mainly caused by the high degrees of freedom and the relatively large measurement noise. The use of discrete cosine transform (DCT) to cluster finite elements has been proposed to reduce the degrees of freedom in inverse computations. However, blurred anatomical alignment and artifacts still present challenges to the interpretation of EIT images. Incorporating prior information into the reconstruction process has been reported to enhance the quality of EIT images. In this contribution, we propose the use of a patient-specific structural prior mask for the DCT-based EIT algorithm. We evaluate the influence of this mask on simulation models with varying ventilation statuses. Our results demonstrate that the structural prior mask preserves the morphological structures of the lungs and avoids blurring of the solution, thereby facilitating EIT image interpretation for clinicians.

Keywords: Biomedical and medical image processing and systems; biomedical system modeling, simulation and visualization; medical imaging and processing; Physiological Model; decision support and control.

1. INTRODUCTION

Electrical impedance tomography (EIT) is a low-cost medical imaging method which visualises the ventilation and the aeration of the regional lung at the bedside. Small alternating stimulation currents are injected through the electrodes attached around the chest (Frerichs et al., 2017, 2012). During inspiration, the expansion of the alveoli lengthens the current pathways, hence increasing the impedance of the lungs tissue. These induced voltage changes are measured by the attached electrodes and then used for EIT image reconstruction, which shows the conductivity changes inside the thorax. EIT shows positive results in scientific and clinical research by reducing ventilator related lung injury (VILI) in mechanical ventilation (Frerichs et al., 2017; Hinz et al., 2003). It is also helpful to clinicians in adjusting the positive end-expiratory pressure (PEEP) setting of the ventilator during the treatment of acute respiratory distress syndrome (ARDS) patients (Zhao et al., 2010). Compared with other imaging methods, e.g., computed tomography (CT), EIT has no radiation involved, which makes it suitable for frequent examinations or long-term monitoring. Because of the nonlinear nature of the relation between conductivity change and boundary voltage measurements, the EIT image reconstruction is an ill-posed inverse problem characterized with high degrees of freedom (Gong et al., 2017).

An EIT algorithm is proposed to solve the inverse problem with the basic functions derived from discrete cosine transformation (DCT) (Schullcke et al., 2016; Chen and Möller, 2020; Chen and Moeller, 2021). With the clustering of the finite elements by the basic functions from DCT, the degrees of freedom of the inverse problem are decreased. However, EIT images still have low spatial resolution, together with blurred anatomical alignment

⋆ This research was partially supported by the German Federal Ministry of Education and Research (MOVE, Grant 13FH628IX6) and H2020 MSCA Rise (#872488 DCPM).

10.1016/j.ifacol.2023.10.476

and reconstruction induced artefacts, which makes them difficult to interpret in clinical settings. The combination of modalities as priors to improve image accuracy is a common concept and can be applied to EIT. Some research groups reported the method in terms of introducing structural prior information into EIT images (Glidewell and Ng, 1995; Vauhkonen et al., 1997; Adler et al., 2009). The results showed improvements in reconstructed images, hence forming a more direct comprehensive insight in EIT image interpretation. Several different approaches were reported to introduce structural priors to the EIT reconstruction process. It is widely applicable to assign known anatomical properties to a predefined area within the finite element model (FEM), e.g., assigning different background conductivity to grouped finite elements (Glidewell and Ng, 1995). A prior can also be integrated by a subset of basic functions, e.g., choosing basic functions derived from the principal eigenvectors of a representative ensemble of expectable conductivity distributions (Vauhkonen et al., 1997).

Patient specific structural priors, e.g., obtained from CT, can also be included into the reconstruction process, thus the EIT reconstructions provide a broader insight into the pathophysiology of the lungs (Schullcke et al., 2016). The applied structural prior could facilitate the superposition of EIT reconstructions of conductivity change and structural images. However, in the DCT approach, it is not clear how the reconstruction is influenced by applying the structural priors from morphological image as a mask to the inverse problem.

The objective of this work is to investigate the influence of the personalised structural prior mask on the EIT reconstructions, particularly using the DCT-based EIT algorithm. Simulations in terms of different ventilation status were conducted. EIT images were reconstructed by the DCT-based EIT algorithm without and with the structural prior mask. The comparison of the EIT reconstruction was conducted to quantitatively analyse the influence.

2. METHODS

2.1 DCT-based EIT reconstruction

The reconstruction process for conductivity variation $\hat{\mathbf{x}}$ in EIT is an ill-posed inverse problem, and accurate reconstruction of conductivity distribution change $\mathbf{x} = \sigma_2 - \sigma_1$ is not linearly related to the measurements of the boundary voltage variation $\mathbf{y} = \mathbf{v}_2 - \mathbf{v}_1$. The EIT reconstruction problem is usually formulated as:

$$\hat{\mathbf{x}} = \text{argmin}_{\mathbf{x}} \left\{ \| F(\mathbf{x}) - \mathbf{y} \|_2^2 + \lambda^2 \| \mathbf{R}\mathbf{x} \|_2^2 \right\} \quad (1)$$

where $\hat{\mathbf{x}}$ is the reconstructed conductivity change, and $\mathbf{F}(x)$ represents the nonlinear model that maps conductivity change $\mathbf{x}$ to boundary voltage measurements $\mathbf{y}$. A regularization parameter $\mathbf{R}$ is introduced to linearize the problem, and λ is a hyperparameter used to control regularization. Various options can be used for $\mathbf{R}$, such as Tikhonov, NOSER, or Laplace. As the conductivity properties of thorax tissue are not homogeneous, a finite element method (FEM) is required.

In EIT, conductivity changes are typically assumed to be small, smooth, and slowly changing. Therefore, the forward model $\mathbf{F}(x)$ can be linearized around a reference conductivity σ^{ref} as $\mathbf{F}(x) \approx \mathbf{J}\mathbf{x}$. The Jacobian matrix $\mathbf{J}$ is a mapping from voltage variations to conductivity change, and it is derived from a background reference σ^{ref} as $J_{i,j} = \frac{\partial y_i}{\partial x_j}\Big| \sigma^{ref}$. The element Ji, j maps small voltage changes at position i of $\mathbf{y}$ to conductivity change of element j within FEM. Within these assumptions, equation (1) can be solved in a linearized form:

$$\hat{\mathbf{x}} = (\mathbf{J}^T\mathbf{J} + \lambda^2\mathbf{R}^T\mathbf{R})^{-1}\mathbf{J}^T\mathbf{y} = \mathbf{B}\mathbf{y} \quad (2)$$

where the matrix $\mathbf{B}$ is the reconstruction matrix. This represents a widely used one-step Gauss-Newton algorithm.

In this research, we introduced the discrete cosine transform (DCT) basic function subset $\mathbf{D}$, which is a subset of cosine functions at varying frequencies, to decrease the degrees of freedom in the EIT inverse problem. A DCT subset is generated as:

$$D(p,q)m,n = \alpha p \alpha_q \cos\frac{(2m+1)p\pi}{2M} \cdot \cos\frac{(2n+1)q\pi}{2N} \quad (3)$$

where p and q are the frequencies of the cosine function at the x-axis and y-axis, respectively. In this research, p and q were chosen as 15 frequencies at either axis. The desired EIT image size has M rows and N columns.

A structural prior mask $\mathbf{P}$ derived from a structural image, such as CT, can be integrated into the EIT reconstruction process by multiplying it with $\mathbf{D}(p,q)$ as follows:

$$C(p,q)_{m,n} = P_{m,n} \cdot D(p,q)_{m,n} \quad (4)$$

The matrix $\mathbf{P}$ specifies the shape of the lungs and may also include other structural details which can be obtained. Using the matrix $\mathbf{D}(p,q)$ (without structural prior) or $\mathbf{C}(p,q)$ (with structural prior), the columns of the basic function subset is calculated as $\mathbf{K}_j^{np} = T(\mathbf{D}(p,q))$ or $\mathbf{K}_j^{p} = T(\mathbf{C}(p,q))$. T is a mapping function assigning each pixel of basic function subset to corresponding FEM elements. An example of $\mathbf{K}_{32}^{np}$ and $\mathbf{K}_{32}^{p}$ $(p = 1, q = 2)$ is depicted in Fig. 1.

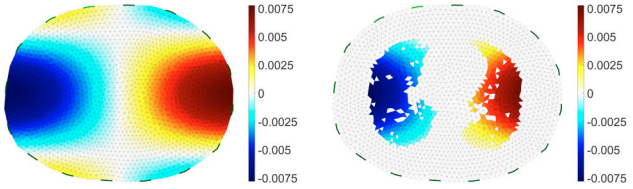

Fig. 1. Visualization of the FEM elements clustered by the column of $\mathbf{K}$: left:$\mathbf{K}_{32}^{np}$; right: $\mathbf{K}_{32}^{p}$.

The Jacobian matrix $\mathbf{J}$ is modified by the subset matrix $\mathbf{K}$ ($\mathbf{K}^{np}$ or $\mathbf{K}^{p}$) as $\mathbf{J}_{DCT} = \mathbf{J} \cdot \mathbf{K}$. Final $\mathbf{J}_{DCT}$ contains only $n_{meas} \times n_{DCT}$ elements which is far less than the finite elements. $\mathbf{J}_{DCT}$ now maps from the voltage variations to the DCT coefficients change. The solution of inverse problem is represented by the change of DCT coefficients $\hat{\mathbf{x}}_{DCT}$:

$$\hat{\mathbf{x}}_{DCT} = (\mathbf{J}_{DCT}^T \mathbf{J}_{DCT} + \lambda^2 \mathbf{R}^T \mathbf{R})^{-1} \mathbf{J}_{DCT}^T \mathbf{y} = \mathbf{B}_{DCT} \mathbf{y} \quad (5)$$

The change of the DCT coefficients $\hat{\mathbf{x}}_{DCT}$ is used to restore the EIT image $\mathbf{H}$ through inverse DCT:

$$\mathbf{H} = \sum_{p=0}^{n_{xDCT}} \sum_{q=0}^{n_{yDCT}} \mathbf{C}(p,q) \cdot \hat{x}_{DCT,j} \quad (6)$$

The general procedures of the DCT-based EIT algorithm are depicted in Fig. 2.

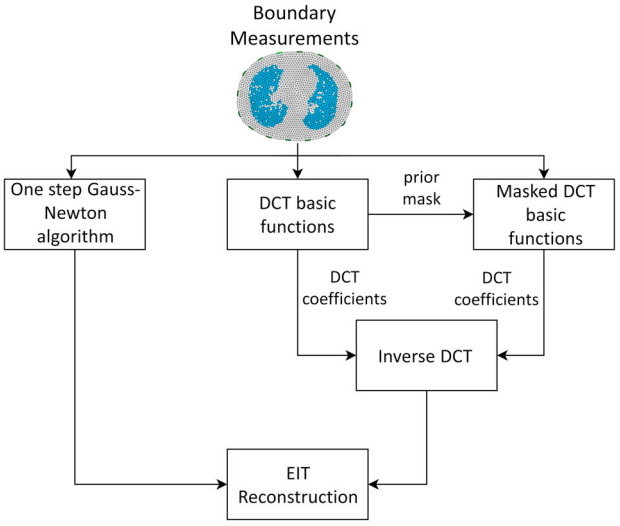

Fig. 2. General procedures of the DCT-based EIT algorithm.

In this contribution, the Tikhonov regularization $\mathbf{R} = \mathbf{I}$ is used for EIT reconstruction. The optimal hyperparameter is chosen when the noise figure (NF) reaches 0.5.

2.2 Simulation data

The numerical simulations to evaluate the influence of patient-specific structural prior mask on EIT reconstructions were conducted using MATLAB R2019a (Mathworks, Natick, MA, USA) with the EIDORS toolbox (Adler and Lionheart, 2006). A FEM was generated from NETGEN using lung and thorax shapes derived from a retrospective CT dataset for the simulations (Schöberl, 1997). At the initial setting of the simulation (i.e., end of expiration), FEM elements not corresponding to lung tissue were assigned a conductivity of $\sigma_{non\text{-}lung}^{initial} = 1$, while elements corresponding to lung tissue were set to a conductivity of $\sigma_{lung}^{initial} = 0.5$. The boundary voltage measurement $\mathbf{v}^{initial}$ was generated with the initial simulation setting and used as a reference for reconstruction. Boundary voltage measurements at end-inspiration were simulated with four different ventilation patterns (see the first row of Fig. 3):

(a) complete lung with homogeneous ventilation;
(b) dorsal right lung with no ventilation;
(c) most ventral and dorsal parts of both lungs with no ventilation;
(d) ventral left lung and dorsal right lung with no ventilation.

For each simulation pattern, the ventilated lung region were simulated by changing the conductivity to $\sigma_{lung}^{vent} = 0.25$. Accordingly, the boundary voltage measurement $\mathbf{v}_i^{vent}$ was generated. 1% white noise was superimposed to the boundary measurement $\mathbf{v}_i^{vent}$ before it was used for reconstruction purpose. A different FEM mesh was implemented in reconstruction to prevent the 'inverse-crime' (Lionheart, 2004). The structural prior masks integrated into the DCT approach were derived from the simulation ground truth.

2.3 Evaluation of the reconstruction

The difference between the reconstructed image and the ground truth is calculated by the pixel-wise ℓ_2-norm of the image differences:

$$\ell_2 \; norm = \sqrt{\sum_{i=1}^{M} \sum_{j=1}^{N} (H_{ij}^{Re} - H_{ij}^{GT})^2} \quad (7)$$

where the $\mathbf{H}^{Re}$ is the EIT reconstruction from DCT approach, $\mathbf{H}^{GT}$ represents the simulation ground truth, ij is the index of each pixel.

Regional behaviour, which in EIT is the pixel values of the reconstructed images, is also investigated. In this contribution, we only considered conductivity decrease in the simulations. By comparing pixel values of the reconstructed images with the pixel value in simulation ground truth, we can categorise the pixels of the reconstructed image into four groups:

- G1: correctly reconstructed conductivity decrease;
- G2: wrongly reconstructed conductivity decrease;
- G3: wrongly reconstructed no conductivity change;
- G4: correctly reconstructed no conductivity change.

G1 and G4 represent the correct conductivity reconstruction, while G2 and G3 the incorrect reconstruction.

3. RESULTS

Figure 3 displays the EIT images generated by the DCT approach for four different simulated patterns. Regions with no conductivity change are shown in black, while regions with decreased conductivity are shown in blue. The first row of the figure shows the ground truth conductivity change implemented in the simulation. The second and third rows illustrate the EIT image reconstructions obtained from the DCT approach without and with a structural prior mask, respectively..

The results of the ℓ_2-norm of the image difference between reconstructed images and the ground truth data are depicted in Fig. 4. Introducing a structural prior to DCT approach resulted in a reduced ℓ_2-norm of image difference compared to the results without a structural prior mask.

Figure 5 shows the fractions of correctly reconstructed pixels (group G1 and G4) and wrongly reconstructed pixels (group G2 and G3). For the images reconstructed using the DCT approach without a structural prior mask, the fractions of correctly reconstructed pixels are: (a) 0.35, (b) 0.27, (c) 0.17, and (d) 0.21. With a structural prior mask,

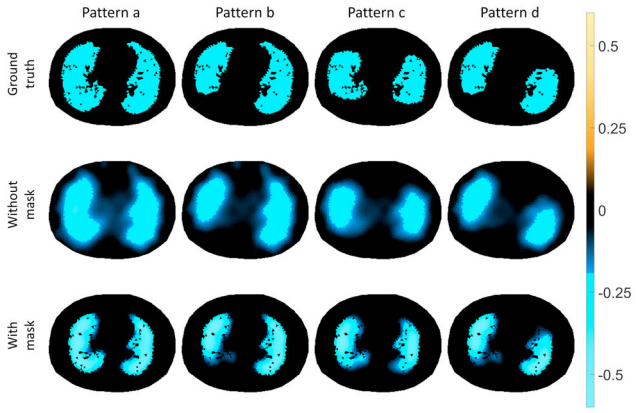

Fig. 3. Ground truth and the EIT reconstructions using DCT approach. First row: different patterns of conductivity change for simulation (ground truth); second row: reconstructions of the conductivity change using DCT approach without a structural prior mask; third row: reconstructions of the conductivity change using DCT approach with a structural prior mask.

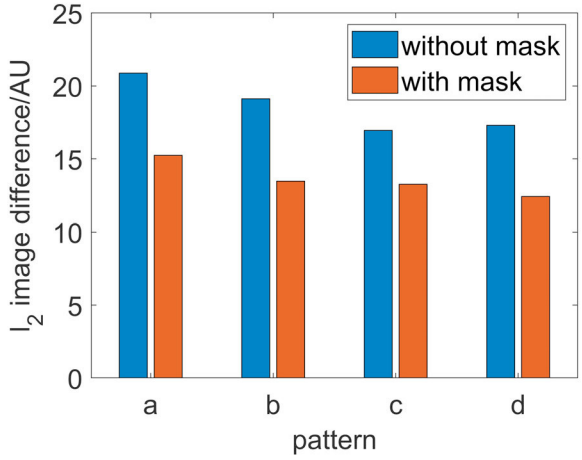

Fig. 4. The ℓ_2-norm of image difference between the respective reconstructions and the ground truth.

these values improve to: (a) 0.65, (b) 0.59, (c) 0.35, and (d) 0.45.

4. DISCUSSION

In this study, we aimed to investigate the impact of a structural prior mask on the accuracy and interpretability of EIT reconstructions using the DCT approach. We simulated four different ventilation patterns and evaluated the reconstructions with and without the prior mask. Overall, the reconstructions using the DCT approach with a prior mask are able to better utilize the structural information and reconstruct the conductivity changes within the lung region, resulting in clearer and more accurate EIT images.

The results demonstrate that the use of a structural prior mask significantly improves the accuracy and interpretability of EIT reconstructions. In Fig. 3, the DCT reconstructions using the structural prior maintain the shape of the lungs, making the overall EIT image much clearer. Artifacts from the reconstruction algorithm at the

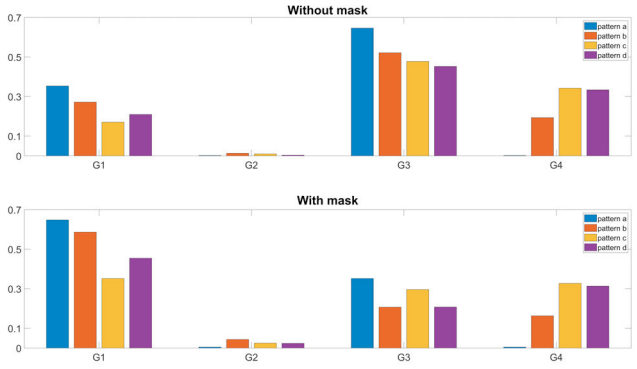

Fig. 5. Fractions of pixel categories based on conductivity changes in reconstructed EIT images: G1 (correctly reconstructed conductivity decrease), G2 (wrongly reconstructed conductivity decrease), G3 (wrongly reconstructed no conductivity change), and G4 (correctly reconstructed no conductivity change). First row: without a structural prior mask; second row: with a structural prior mask.

non-lung regions are also prevented (compare the second row and the third row in Fig. 3). This will also facilitate the development of a comprehensive insight into the pathophysiology of lungs in clinical settings, since regional behaviour of the lungs could be directly correlated with the morphological structures. In addition, introducing the structural prior mask is a simple and direct procedure in terms of mapping function. With the prior mask, the correctly reconstructed pixels (see G1 in Fig. 5) in the EIT image were increased, hence decreasing the ℓ_2-norm of the image difference (see Fig. 4). It also reduced the fraction of pixels which wrongly state no change in the conductivity (see G3 in Fig. 5), mainly due to the constraint of reconstruction within the lung area. Meanwhile, the DCT approach with prior mask also slightly increased the fraction of the wrongly reconstructed pixels with decreased conductivity (see G2 in Fig. 5).

It is worth noting that all the structural prior masks implemented in the evaluation come directly from the simulation ground truth, which means the structural priors are accurate. This is crucial when implementing prior mask for the DCT approach. An inaccurate structural prior mask, i.e., when it does not comply with the current patient status, could introduce a risk in terms of misleading interpretation of the results, compromising the diagnosis in clinical settings (Chen and Moeller, 2021; Chen et al., 2022). It is necessary that the implemented structural prior mask in the DCT approach is checked regularly to maintain its accuracy. Meanwhile, in EIT various sources of artefacts, e.g., patient movement and electrode connection variability, produce a strong voltage signal. There might exist a risk that these sources of artifacts will be interpreted as the conductivity change within the lung region in the reconstruction due to the implementation of the prior mask.

One of the limitations of this research is that the influence of the structural prior mask is only evaluated by simulations. Further research with clinical data should be carried out. The comparison is only between the DCT approach with and without a structural prior mask. There exists

other methods to implement a prior information to DCT approach, e.g., through a personalised regularization. This method should also be included in future research. The FEM used for the simulations has the same thorax shape from a retrospective dataset. More thorax shape should be included in the future evaluation to test the robustness of this method. Nevertheless, different status of the lungs were investigated in this preliminary study, which represent the patient-specificity. Another concern is that the computation of the DCT approach is very intensive, which might jeopardise the real-time analysis of the EIT images. However, with a specialised algorithm the computational intensity can be reduced significantly (Chase and Pretty, 2002). This will allow it to be performed in real-time on typical clinical hardware.

Nevertheless, through the evaluation with the simulation models, when an accurate structural prior mask is implemented, the EIT reconstruction benefits from the improved interpretability. It is promising that the DCT approach with prior mask facilitates the superposition of data obtained from EIT with the structural details from other morphological imaging methods, therefore it might be helpful to clinicians in terms of EIT image interpretation.

5. CONCLUSION

The influence of the structural prior mask was evaluated in terms of simulation models. In conclusion, the anomalies of ventilation, i.e., different conductivity distributions, can be correlated with respected structural information from other morphological imaging methods by implementing a structural prior mask. Thus, the EIT reconstruction accuracy is improved. The research suggests that the DCT approach with a structural prior mask might be a step forward to improve diagnostic accuracy using the EIT imaging method.

REFERENCES

Adler, A., Arnold, J.H., Bayford, R., Borsic, A., Brown, B., Dixon, P., Faes, T.J., Frerichs, I., Gagnon, H., Garber, Y., Grychtol, B., Hahn, G., Lionheart, W.R., Malik, A., Patterson, R.P., Stocks, J., Tizzard, A., Weiler, N., and Wolf, G.K. (2009). GREIT: A unified approach to 2D linear EIT reconstruction of lung images. *Physiological measurement*, 30(6), S35–55.

Adler, A. and Lionheart, W.R.B. (2006). Uses and abuses of EIDORS: An extensible software base for EIT. *Physiological Measurement*, 27(5), S25–S42. doi: 10.1088/0967-3334/27/5/S03.

Chase, J.G. and Pretty, C. (2002). Software defined QCIF simple profile MPEG-4 for portable devices using dynamically reconfigurable DSP. *Computer Standards & Interfaces*, 24(5), 453–472. doi:10.1016/S0920-5489(02)00069-7.

Chen, R. and Moeller, K. (2021). Redistribution Index – Detection of an Outdated Prior Information in the Discrete Cosine Transformation-based EIT Algorithm. In *2021 43rd Annual International Conference of the IEEE Engineering in Medicine Biology Society (EMBC)*, 3693–3696. doi:10.1109/EMBC46164.2021.9630567.

Chen, R. and Möller, K. (2020). Global inhomogeneity index evaluation of a DCT-based EIT lung imaging. *Current Directions in Biomedical Engineering*, 6(3), 36–39. doi:10.1515/cdbme-2020-3010.

Chen, R., Rupitsch, S.J., and Moeller, K. (2022). Influence of hyperparameter on the Untrue Prior Detection in Discrete Transformation-based EIT Algorithm. In *2022 44th Annual International Conference of the IEEE Engineering in Medicine & Biology Society (EMBC)*, 580–583. doi:10.1109/EMBC48229.2022.9871293.

Frerichs, I., Achtzehn, U., Pechmann, A., Pulletz, S., Schmidt, E.W., Quintel, M., and Weiler, N. (2012). High-frequency oscillatory ventilation in patients with acute exacerbation of chronic obstructive pulmonary disease. *Journal of critical care*, 27(2), 172–81.

Frerichs, I. et al. (2017). Chest electrical impedance tomography examination, data analysis, terminology, clinical use and recommendations: Consensus statement of the TRanslational EIT developmeNt stuDy group. *Thorax*, 72(1), 83–93. doi:10.1136/thoraxjnl-2016-208357.

Glidewell, M. and Ng, K.T. (1995). Anatomically constrained electrical impedance tomography for anisotropic bodies via a two-step approach. *IEEE Transactions on Medical Imaging*, 14(3), 498–503. doi: 10.1109/42.414615.

Gong, B., Schullcke, B., Krueger-Ziolek, S., Vauhkonen, M., Wolf, G., Mueller-Lisse, U., and Moeller, K. (2017). EIT imaging regularization based on spectral graph wavelets. *IEEE transactions on medical imaging*, 36(9), 1832–1844.

Hinz, J., Neumann, P., Dudykevych, T., Andersson, L.G., Wrigge, H., Burchardi, H., and Hedenstierna, G. (2003). Regional ventilation by electrical impedance tomography: A comparison with ventilation scintigraphy in pigs. *Chest*, 124(1), 314–22.

Lionheart, W.R.B. (2004). EIT reconstruction algorithms: Pitfalls, challenges and recent developments. *Physiological Measurement*, 25(1), 125. doi:10.1088/0967-3334/25/1/021.

Schöberl, J. (1997). NETGEN An advancing front 2D/3D-mesh generator based on abstract rules. *Computing and Visualization in Science*, 1(1), 41–52. doi: 10.1007/s007910050004.

Schullcke, B., Gong, B., Krueger-Ziolek, S., Soleimani, M., Mueller-Lisse, U., and Moeller, K. (2016). Structural-functional lung imaging using a combined CT-EIT and a discrete cosine transformation reconstruction method. *Scientific reports*, 6, 25951.

Vauhkonen, M., Kaipio, J., Somersalo, E., and Karjalainen, P. (1997). Electrical impedance tomography with basis constraints. *Inverse problems*, 13(2), 523.

Zhao, Z., Steinmann, D., Frerichs, I., Guttmann, J., and Moller, K. (2010). PEEP titration guided by ventilation homogeneity: A feasibility study using electrical impedance tomography. *Critical Care*, 14(1), R8.